HYDROTHERMAL ALTERATION AND WHOLE ROCK GEOCHEMISTRY OF THE TAUHARA GEOTHERMAL FIELD: TRADITIONAL VERSUS RAPID TECHNIQUES

Kate Mauriohooho[1], Shaun L.L. Barker[1], Andrew J. Rae[2] and Mark P. Simpson[2]

[1]School of Science & Engineering, The University of Waikato, Private Bag 3105

Hamilton 3240, New Zealand

[2]GNS Science, Wairakei Research Centre, Private Bag 2000, Taupo, New Zealand

[1]km179@students.waikato.ac.nz, sbarker@waikato.ac.nz

[2]a.rae@gns.cri.nz, m.simpson@gns.cri.nz

Keywords: *geothermal, alteration mineralogy, XRF, pXRF, geochemistry, SWIR*

ABSTRACT

Established practices that characterise the geology of geothermal fields involve primary (host rock) and secondary (alteration) mineral identification using visual description of cuttings and core, optical microscopy and x-ray diffraction (XRD). More recently, new technologies such as short wave infrared (SWIR) and portable x-ray fluorescence (pXRF) have emerged (primarily driven by demand from the mineral exploration industry) that can obtain mineralogical and geochemical information relevant to geothermal industry and research.

Whole rock geochemistry is not routinely carried out during geothermal well logging due to cost and time constraints. For this reason, pXRF data, which can be obtained rapidly and inexpensively, is evaluated against traditional lab-based x-ray fluorescence methods (XRF). Three geothermal wells (TH9, TH10 and TH12) located across the Tauhara Geothermal Field were examined and the hydrothermal alteration mineralogy and whole rock geochemistry of each assessed.

The results presented here demonstrate that pXRF data can be used to distinguish lithologies based on immobile element concentrations (e.g. Y, Zr, and Nb). In addition, Si and Sr show significant differences between lithological units. Therefore, immobile element concentrations and ratios may be useful for distinguishing boundaries between lithological units that are otherwise difficult to determine by mineralogy and petrography alone. Higher permeability zones accompanied by more intense hydrothermal alteration, is reflected in elevated concentrations of fluid mobile elements such as Ba, K, Ca, As, Rb and Pb. Comparison between traditional lab-based XRF (fused and press powder discs) and portable XRF on cuttings shows generally excellent correlation (r_s>0.8) between the two methods for As, Ba, Ca, K, Nb, Rb, Sr, Y, Zr. However Al, Cu, Mn, Mo, Pb, S, Si, Th, Cr, Sb, Sn, Ta, Zn are not as well correlated between the two methods (r_s<0.7). Thus pXRF is likely an efficient and cost effective technique for distinguishing lithology changes and hydrothermal alteration of host rocks particularly where a preliminary and rapid assessment is required.

This study also compares traditional x-ray diffraction data with Terraspec® data (a type of SWIR instrument) to determine its effectiveness in identifying hydrothermal alteration minerals when applied to cuttings from geothermal wells. Interpretation of SWIR spectral profiles have identified smectite, illite-smectite, illite, chlorite, epidote and calcite, reflecting both argillic and propylitic alteration types. Below 1040 mRF in TH12, SWIR spectra suggest illite-smectite or smectite in contrast to XRD which indicates illite, therefore clay separate analysis of these samples is required for verification.

1. INTRODUCTION

1.1 Background

In hydrothermal systems, a heat source circulates fluid at different temperatures and pressures, through a system of fractures, faults and permeable host rocks where the fluid alters the rock in the process. These interactions between fluid and rock lead to changes in the host rock minerals to form secondary minerals, including clay minerals (hydrothermal alteration minerals) some of which are broadly temperature dependent (Browne, 1970). Thus certain minerals and/or mineral assemblages are formed under specific temperature ranges and conditions, such as permeability, pH/fluid composition, pressure and duration of interaction. These minerals can also be influenced by host rock composition (Browne and Ellis, 1970; Browne, 1978). Changes in alteration mineral assemblages can be used to locate hotter areas, related to up-flow zones in active hydrothermal systems (i.e. geothermal fields).

Here we examine the hydrothermal alteration mineralogy and whole rock geochemistry in three geothermal wells (TH9, TH10, TH12) from the Tauhara Geothermal Field in the Taupo Volcanic Zone. Previous work on the Wairakei-Tauhara system has been completed by a number of authors (Grange, 1937; Grindley, 1965, 1974, 1982; Steiner, 1977; Healy, 1967; Browne, 1970; Rosenberg et al., 2010; Bignall et al., 2010, Bromley et al., 2010). This paper presents results from portable x-ray fluorescence (pXRF) and short wave infrared (SWIR) survey using Terraspec® that are then compared to results from traditional lab-based XRF and x-ray diffraction (XRD) from relevant GNS well reports (TH9, TH10, TH12). From the results presented, early inferences and degrees of correlation are considered.

2. GEOLOGICAL SETTING

2.1 Location

The Tauhara Geothermal Field has a total surface area of 50 km² (Rosenberg et al., 2010) and is located within the Taupo Volcanic Zone in the central North Island, New Zealand, 3 km northeast of Lake Taupo (Fig. 1). The Waikato River borders the western side of the Tauhara field and Mt Tauhara, an extinct dacite volcano, is on the southeast (Steiner, 1977) (Fig. 2). It is classed as a high enthalpy resource, with a natural energy output at 110 Mw (Bibby et al., 1995). To the south-east of Wairakei is the Tauhara

geothermal resource. Although both fields have separate upflow zones previous studies have documented a hydrological connection between the two fields, with pressure drawdown at Tauhara linked to long-term production at Wairakei (Hunt & Graham, 2009; Milloy & Wei Lim, 2012).

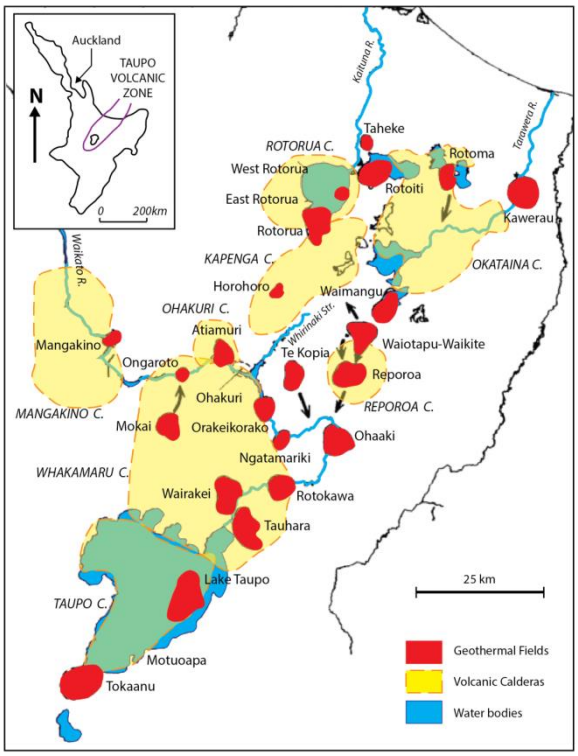

Figure 1: Location map of Tauhara Geothermal Field and other geothermal fields of the Taupo Volcanic Zone (after Bibby et al., 1995). Capitalised labels refer to indicated calderas.

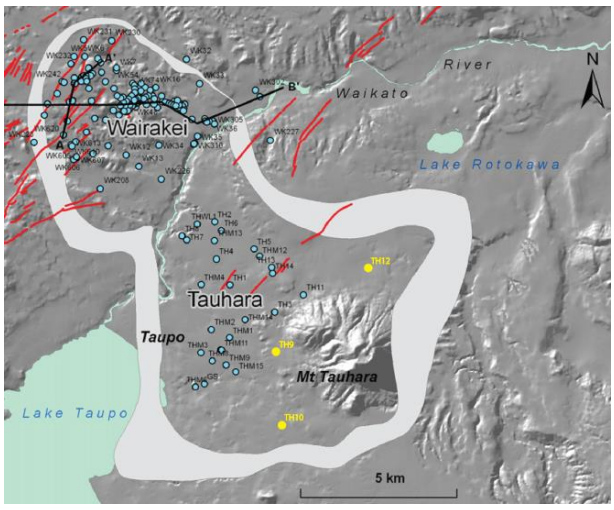

Figure 2: Map of the Tauhara Geothermal Field (southeast) as part of the Wairakei-Tauhara geothermal system (after Rosenberg et al., 2009). TH9, TH10 and TH12 geothermal wells shown by yellow circles. Resistivity boundary (to a depth of 500 m) is delineated by the light grey shaded area.

2.2. Stratigraphy

The regional geology was illustrated by Grange (1955). Grindley (1965) further outlined the geology of the Wairakei geothermal field. The Wairakei-Tauhara area mostly consists of pyroclastic fall and flow units outcropping on the surface. Extensive drilling at Wairakei and Tauhara from 2006 to 2013 resulted in additional geological information, prompting stratigraphy and geology reviews such as those by Rosenberg et al., (2009) and Bignall et al., (2010) (Fig. 3).

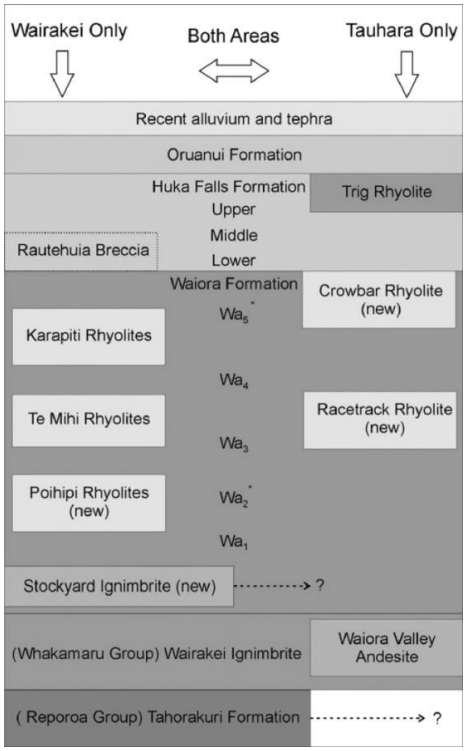

Figure 3: Stratigraphic units of the Wairakei and Tauhara Geothermal Fields (Rosenberg et al., 2009).

From top to bottom, the shallow stratigraphy of Tauhara includes: Superficial Alluvium and Tephra (Rosenberg et al., 2010); underlain by the Oruanui Formation a sequence of tuffs and ignimbrites that are products of a single eruption from the former Lake Taupo 26,500 years ago (Wilson, 1993; Wilson, 2001 ; Bignall et al., 2010); and the Huka Falls Formation (HFF) which is subdivided into the Upper, Middle and Lower Huka Falls Formation members. The Upper and Lower members mainly consist of fine-grained lacustrine sedimentary rocks (mudstone, siltstone, sandstone) that behave as acquicludes but are locally interbedded with rhyolites (e.g. Trig Rhyolite; Grindley, 1965). The Middle HFF on the other hand encompasses pumiceous tuff and conglomerate from reworked ignimbrites and because of its high permeability it functions as an acquifer. The HFF examined as a whole formation is also important hydrologically as it acts as an acquitard between hot fluid in the Waiora Formation and shallow groundwater (Bignall et al., 2010).

Underlying HFF is the Waiora Formation that is split into 5 members as described by Grindley (1965): Wa5 is ignimbrite and tuff, Wa3 and Wa4 is breccia, tuff, sandstone and siltstone inter-bedded together, Wa2 is siltstone and basal member Wa1 is non-welded/welded ignimbrite that is also referred to as Waiora Ignimbrite. These members are not present continuously across Wairakei and Tauhara

Fields. Rosenberg et al. (2009) proposed a simplification of the Waiora Formation subdivision and grouped members Wa3 and Wa4 into Wa3-4 member which is the classification currently in use. The Waiora Formation is laterally interbedded with rhyolite bodies such as the Crowbar and Racetrack Rhyolites.

Underlying the Waiora Formation is the Wairakei Ignimbrite from the Whakamaru Group (Rosenberg et al., 2009; Bignall et al., 2010), which is crystal-rich and moderately welded. In some wells the Wairakei Ignimbrite is absent (TH9, TH10), but is present in TH12 suggesting that the Wairakei Ignimbrite is geometrically controlled by horst and graben fault structures (Rosenberg et al., 2009; Bignall et al., 2010). Below 1000 mRSL, the deeper stratigraphy of Wairakei-Tauhara is dominated by rhyolite and andesite lavas that is further underlain by volcaniclastic and sedimentary units of the Tahorakuri Formation (Gravley et al., 2006, Bignall et al., 2010). The underlying Jurassic greywacke basement rocks, intersected elsewhere in the Taupo Volcanic Zone, such as in Rotokawa, Ohaaki, Ngatamariki and Kawerau geothermal fields, have been intersected by only one well in the whole Wairakei-Tauhara region (well TH17, Northeastern boundary of the Tauhara Field).

2.3. Hydrothermal alteration

Hydrothermal alteration studies reveal increased alteration intensity with depth. The presence of epidote indicates temperatures in excess of 250ºC (Rosenberg et al., 2009; 2010). The Oruanui Formation and HFF are affected by an argillic alteration assemblage (smectite, calcite ± pyrite, ± illite-smectite) at shallow levels. Interlayered illite-smectite, hydrothermal quartz, calcite and pyrite followed by minor illite, chlorite and epidote indicate an increase in alteration intensity. As depth increases propylitic alteration becomes the dominant style represented by chlorite, quartz, epidote, albite, adularia, wairakite and titanite. Rosenberg et al (2009) and Bignall et al (2010) state that the propylitic assemblage (adularia, albite) on the western side of the Wairakei-Tauhara system has been overprinted by an illite-calcite assemblage indicating a decrease in temperature or pH of the fluid, although this overprint is not seen on the eastern side of the field.

3. SAMPLING AND ANALYTICAL TECHNIQUES

Three geothermal wells (TH9, TH10, TH12) were selected for detailed portable X-ray fluorescence (pXRF) and short-wave infrared (SWIR) analyses. Samples of rock cuttings were collected every 20 m down well; where no rock cuttings at the required interval existed, a sample from the closest available interval was taken. Samples were also taken 5 – 10 m either side of lithological boundaries and at least 20 m beneath casing points. A total of 301 samples were selected for whole rock geochemistry analysis by pXRF and mineral identification by SWIR spectroscopy in order to determine hydrothermal alteration minerals, and the geochemistry of the rock types and alteration to distinguish lithology. Both techniques collect data rapidly and require no sample preparation and thus a far greater number of samples can be analysed compared to traditional XRD and XRF.

Sample preparation for pXRF required a small sample (1/2 teaspoon of cuttings) to be put into an assembled sample cup, with a thin Mylar film. An Olympus 50 KV Handheld XRF Analyzer was mounted in a stand and concentrations of major and trace elements recorded by Innov-X Delta Advanced PC software. Elements analysed; Nd, Pr, Ce, La, Ba, Y, Al, Si, P, S, Cl, K, Ca, Ti, V, Cr, Mn, Fe, Co, Ni, Cu, Zn, As, Se, Rb, Sr, Zr, Nb, Mo, Ag, Cd, Sn, Sb, Ta, W, Au, Hg, Pb, Bi, Th, U. Scans took one minute per sample. Sample preparation for SWIR only required that the cuttings be dry. Data was collected using a TerraSpec® 4 Hi-Res instrument with 3 scans collected per sample, each scan taking 10 s. Interpretations were made using The Spectral Geologist (TSG®) software.

In order to check the accuracy of the pXRF results, 45 samples (15 from each well) representative of the different formations were selected for traditional lab-based XRF. Major elemental oxides were determined on fused disks and trace elements verified on pressed pellets. Elemental oxides and trace elements analysed; Na_2O, MgO, Al_2O_3, SiO_2 P_2O_5, K_2O, CaO, TiO_2, MnO, Fe_2O_3, S, Cl, V, Cr, Co, Ni, Cu, Zn, Ga, Ge, As, Se, Br, Rb, Sr, Y, Zr, Nb, Mo, Sn, Sb, Te, Ba, La, Ce, Nd, Hf, Ta, Tl, Pb, Bi, Th, U.

4. pXRF RESULTS

4.1. Comparison of traditional and portable XRF methods

Table 1 and Figure 4 illustrate the comparison between elements in 45 samples that were analysed by both pXRF and lab-based XRF. It must be emphasized that the pXRF data was collected straight on the "raw" cuttings (individual chips ~ 3 to 5 mm) meaning no preparation. The lab-based XRF data were collected on cuttings that had been crushed to a fine powder using a ring mill. The drillcuttings used in pXRF and lab XRF were also not cleaned of drillbit scrapings or LCM, only drilling mud. Nevertheless, comparison of the two techniques reveals that many elements show strong, positive correlations (Spearman correlation coefficient (r_s) values > +0.8). For instance, Ba (r_s = 0.93) and Zr (r_s = 0.89) are both well correlated (Table 1). The presence of outliers can potentially skew correlations hence the Spearman rank correlation method was used throughout this paper as it is more robust against outliers (Rollinson, 1993) (Fig, 4). For example, Pb has a correlation coefficient of r = 0.93 using the Pearsons product moment correlation method it is sensitive to outliers, whereas the Spearman rank correlation method gives a more reliable correlation coefficient for Pb of r_s = 0.68.

Yttrium and Rb are also well correlated (0.89) whereas Al is poorly correlated (0.17; Table 1: Fig. 4). Other elements with strong positive correlations of at least 0.80 are As, Ba, Ca, K, Nb, Rb, Sr, Y, and Zr. Ti has a +1 correlation but the basis of this relies on detection by pXRF in only four samples. Elements with moderate correlation (r_s = 0.5 – 0.8) are Mn, Mo, Pb, S, Si, Zn and Fe. Elements showing a lack of correlation (r_s < 0.5) are Al, Cr, Cu, Sb, Ta and Th. Sn has a perfect negative linear relationship at -1, yet again is based on detection in only three samples by pXRF. This suggests that pXRF is somewhat reliable in measuring the concentration of many elements (As, Ba, Ca, K, Nb, Rb, Sr, Y, Zr, Mn, Mo, Pb, S, Si, Zn, Fe), but is not as effective for other elements (Al, Cr, Cu, Sb, Ta, Th).

Piercey and Devine (2013) found excellent correlation between traditional and portable XRF for S, K_2O, CaO, TiO_2, MnO, Fe_2O_3, Co, Cu, Pb, Rb, Sr, Ba, Zr, Nb, U, As and Mo; moderate correlation for Aluminum (Al_2O_3), SiO_2, and Zn and poor correlation for MgO, P_2O_5, V, Cr, and Ni.

Table 1. Lab based XRF and portable XRF correlation matrix (Spearman method) of 13 selected elements.

Spearman	Al_ppm	Al2O3_pct	As_ppm	As-lab	Ba_ppm	Ba-lab	Ca_ppm	CaO_pct	Fe_ppm	Fe2O3_pct	K_ppm	K2O_pct	Nb_ppm	Nb-lab	Pb_ppm	Pb-lab	Rb_ppm	Rb-lab	Si_ppm	SiO2_pct	Sr_ppm	Sr-lab	Y_ppm	Y-lab	Zr_ppm	Zr-lab
Al_ppm	1	0.17	-0.10	-0.26	-0.10	-0.04	-0.03	0.01	0.04	-0.01	0.15	-0.17	-0.03	-0.03	-0.07	-0.25	0.08	-0.09	0.26	-0.01	0.17	0.04	0.17	0.12	0.34	0.20
Al2O3_pct	0.17	1	0.067	-0.21	-0.45	-0.39	0.37	0.60	0.66	0.51	-0.36	-0.29	-0.38	-0.35	0.15	-0.09	-0.33	-0.33	-0.51	-0.65	0.36	0.56	-0.32	-0.29	-0.31	-0.30
As_ppm	-0.10	0.07	1	0.86	-0.39	-0.33	0.35	0.23	0.16	0.19	-0.39	-0.37	-0.11	-0.14	0.37	0.19	-0.03	-0.33	0.04	-0.35	0.22	0.11	0.14	0.06	0.07	0.02
As-lab	-0.26	-0.21	0.86	1	0.12	0.14	-0.21	-0.28	-0.14	-0.19	0.08	0.12	0.21	0.24	0.27	0.43	0.23	0.17	0.16	0.15	-0.23	-0.29	0.20	0.31	0.17	0.24
Ba_ppm	-0.10	-0.45	-0.39	0.12	1	0.93	-0.57	-0.57	-0.71	-0.68	0.74	0.75	0.61	0.70	-0.12	0.29	0.67	0.71	0.34	0.53	-0.55	-0.51	0.54	0.59	0.51	0.60
Ba-lab	-0.04	-0.39	-0.33	0.14	0.93	1	-0.52	-0.53	-0.52	-0.58	0.76	0.79	0.61	0.72	-0.05	0.36	0.70	0.73	0.38	0.44	-0.49	-0.50	0.60	0.65	0.59	0.66
Ca_ppm	-0.03	0.37	0.35	-0.21	-0.57	-0.52	1	0.83	0.46	0.67	-0.50	-0.49	-0.41	-0.55	0.26	-0.04	-0.37	-0.45	-0.47	-0.69	0.61	0.63	-0.22	-0.32	-0.35	-0.44
CaO_pct	0.01	0.60	0.23	-0.28	-0.57	-0.53	0.83	1	0.54	0.63	-0.49	-0.51	-0.53	-0.62	0.08	-0.08	-0.46	-0.50	-0.51	-0.79	0.60	0.71	-0.37	-0.41	-0.48	-0.56
Fe_ppm	0.04	0.66	0.16	-0.14	-0.71	-0.52	0.46	0.54	1	0.71	-0.57	-0.49	-0.41	-0.41	0.25	-0.03	-0.63	-0.61	-0.44	-0.65	0.47	0.55	-0.27	-0.28	-0.33	-0.33
Fe2O3_pct	-0.01	0.51	0.19	-0.19	-0.68	-0.58	0.67	0.63	0.71	1	-0.60	-0.61	-0.61	-0.64	0.20	-0.03	-0.63	-0.65	-0.50	-0.73	0.54	0.66	-0.34	-0.39	-0.47	-0.50
K_ppm	0.15	-0.36	-0.39	0.08	0.74	0.76	-0.50	-0.49	-0.57	-0.60	1	0.81	0.62	0.53	-0.05	0.25	0.82	0.73	0.66	0.52	-0.61	-0.66	0.54	0.49	0.57	0.48
K2O_pct	-0.17	-0.29	-0.37	0.12	0.75	0.79	-0.49	-0.51	-0.49	-0.61	0.81	1	0.64	0.63	-0.15	0.28	0.79	0.90	0.34	0.46	-0.73	-0.68	0.43	0.49	0.45	0.51
Nb_ppm	-0.03	-0.38	-0.11	0.21	0.61	0.61	-0.41	-0.53	-0.41	-0.61	0.62	0.64	1	0.84	0.08	0.36	0.62	0.53	0.46	0.55	-0.53	-0.62	0.78	0.68	0.76	0.72
Nb-lab	-0.03	-0.35	-0.14	0.24	0.70	0.72	-0.55	-0.62	-0.41	-0.64	0.53	0.63	0.84	1	-0.04	0.36	0.54	0.56	0.31	0.50	-0.56	-0.58	0.75	0.82	0.74	0.86
Pb_ppm	-0.07	0.15	0.37	0.27	-0.12	-0.05	0.26	0.08	0.25	0.20	-0.05	-0.15	0.08	-0.04	1	0.68	0.02	-0.21	0.04	-0.28	0.15	0.12	0.33	0.19	0.16	0.02
Pb-lab	-0.25	-0.09	0.19	0.43	0.29	0.36	-0.04	-0.08	-0.03	-0.03	0.25	0.28	0.36	0.36	0.68	1	0.28	0.21	0.06	-0.02	-0.22	-0.15	0.45	0.48	0.29	0.34
Rb_ppm	0.08	-0.33	-0.03	0.23	0.67	0.70	-0.37	-0.46	-0.63	-0.63	0.82	0.79	0.62	0.54	0.02	0.28	1	0.89	0.50	0.45	-0.47	-0.58	0.49	0.49	0.58	0.52
Rb-lab	-0.09	-0.33	-0.33	0.17	0.71	0.73	-0.45	-0.50	-0.61	-0.65	0.73	0.90	0.53	0.56	-0.21	0.21	0.89	1	0.27	0.48	-0.59	-0.60	0.30	0.41	0.36	0.46
Si_ppm	0.26	-0.51	0.04	0.16	0.34	0.38	-0.47	-0.51	-0.44	-0.50	0.66	0.34	0.46	0.31	0.04	0.06	0.50	0.27	1	0.61	-0.34	-0.62	0.47	0.30	0.56	0.33
SiO2_pct	-0.01	-0.65	-0.35	0.15	0.53	0.44	-0.69	-0.79	-0.65	-0.73	0.52	0.46	0.55	0.50	-0.28	-0.02	0.45	0.48	0.61	1	-0.61	-0.79	0.27	0.23	0.39	0.36
Sr_ppm	0.17	0.36	0.22	-0.23	-0.55	-0.49	0.61	0.60	0.47	0.54	-0.61	-0.73	-0.53	-0.56	0.15	-0.22	-0.47	-0.59	-0.34	-0.61	1	0.87	-0.32	-0.42	-0.34	-0.41
Sr-lab	0.04	0.56	0.11	-0.29	-0.51	-0.50	0.63	0.71	0.55	0.66	-0.66	-0.68	-0.62	-0.58	0.12	-0.15	-0.58	-0.60	-0.62	-0.79	0.87	1	-0.41	-0.46	-0.49	-0.46
Y_ppm	0.17	-0.32	0.14	0.20	0.54	0.60	-0.22	-0.37	-0.27	-0.34	0.54	0.43	0.78	0.75	0.33	0.45	0.49	0.30	0.47	0.27	-0.32	-0.41	1	0.89	0.83	0.80
Y-lab	0.12	-0.29	0.06	0.31	0.59	0.65	-0.32	-0.41	-0.28	-0.39	0.49	0.49	0.68	0.82	0.19	0.48	0.49	0.41	0.30	0.23	-0.42	-0.46	0.89	1	0.79	0.88
Zr_ppm	0.34	-0.31	0.07	0.17	0.51	0.59	-0.35	-0.48	-0.33	-0.47	0.57	0.45	0.76	0.74	0.16	0.29	0.58	0.36	0.56	0.39	-0.34	-0.49	0.83	0.79	1	0.89
Zr-lab	0.20	-0.30	0.02	0.24	0.60	0.66	-0.44	-0.56	-0.33	-0.50	0.48	0.51	0.72	0.86	0.02	0.34	0.52	0.46	0.33	0.36	-0.41	-0.46	0.80	0.88	0.89	1

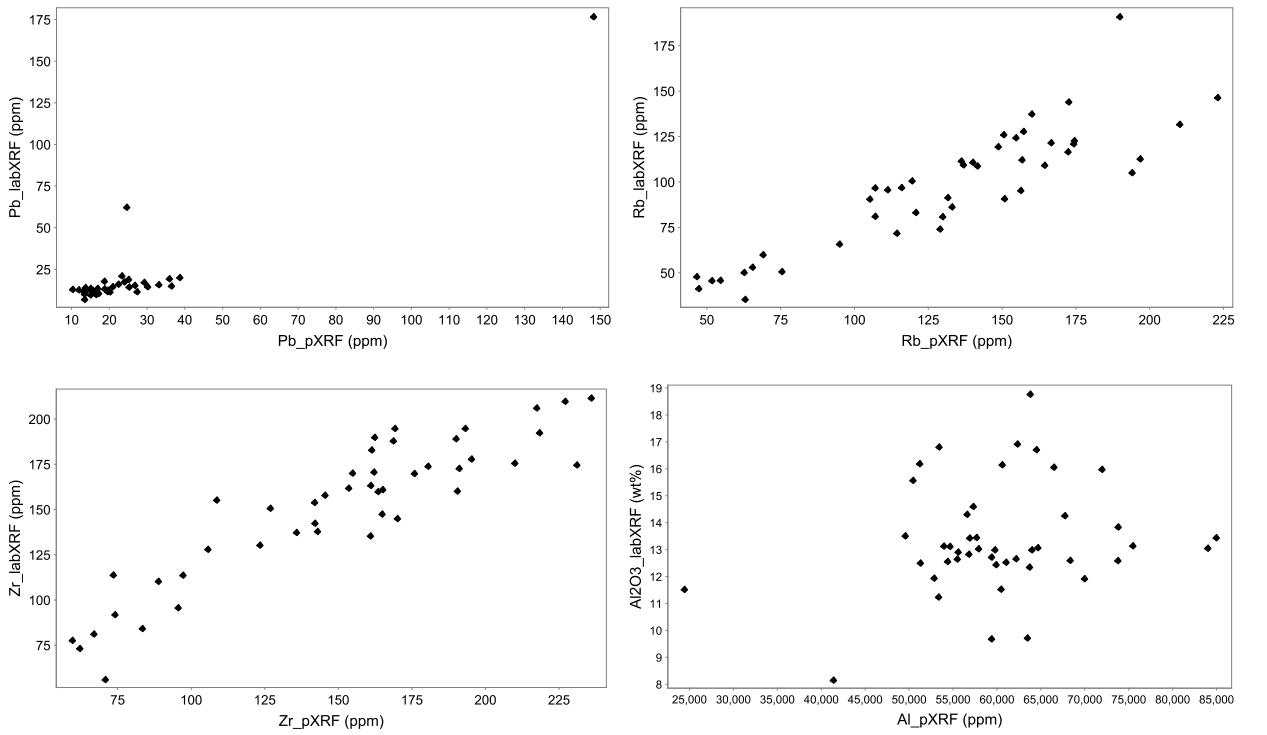

Figure 4: Four correlation plots of elements (Pb, Zr, Rb, Al) showing the correlation between the lab based technique (y-axis) and portable technique (x-axis). A poor correlation is seen for Al.

This suggests that the poor correlations we found between pXRF and laboratory XRF for S and Mo may be related to low Mo concentrations and/or the fact that in our study the pXRF data was collected from cuttings rather than the powdered rock used in Piercey and Devine's (2013) study.

4.2. TH9 well

Barium concentrations increase with depth from approximately 1000-2400 ppm to the base of the Waiora Formation. Yttrium concentrations increase from ~ 30 ppm to ~ 50 ppm between 440 and 480 m with another minor change in concentration also occurring at approximately 900 m, which correlates with the logged transition between the Waiora Formation and the Waiora Ignimbrite (Fig. 5a). Potassium increases with depth from 0 to 900 m, and then remains approximately constant at around 2500 ppm to the bottom of the well. Calcium concentrations are relatively constant at ~ 1.5 wt%, but concentrations as high as 7 wt% occur at ~ 840-860 mRF which are likely related to an increased abundance of hydrothermal calcite. This change is also shown in the well logs from 835-860 mRF. An increase in Ca concentration occurs between 1.5 % and 2.5 % towards the bottom of TH9. Rb concentrations are variable, but show an increase in average concentration from ~ 100 in the Waiora Formation to 130 ppm in the Waiora 1 ignimbrite (Wa1). Arsenic displays constant concentrations of ~13 ppm, but outliers as high as 150 ppm are seen within and below the Huka Falls Formation and at the bottom of TH9 which correlate with recognised hydrothermal feed zones.

4.3. TH10 well

Barium, Y, Si, K, Ca, Fe, Rb, Sr, Zr and Nb all show a clear change in concentration between 1180 and 1200m, which is ~ 85 m above the logged transition between the Waiora 1 ignimbrite (Wa1) and a lithic-crystal breccia (Fig. 5b). Potassium and Ca also seem to generally correlate with formation boundaries down hole. Rubidium also shows other distinct changes in concentration down hole which generally correlate with logged formation boundaries (Fig. 5b). However, some distinct Rb changes occur which do not appear to correlate with recognised formation boundaries. Sulfur displays elevated concentrations at the top of the Crowbar Rhyolite Lava and Huka Falls Formation, and is below detection limit for most samples within the well. Arsenic is elevated at the base of the Huka Falls Formation and minor increases around hydrothermal feed zones are also measured.

4.4. TH12 well

Barium is widely scattered but generally increases in concentration with depth. Yttrium shows significant variability between 20 and 60 ppm, with changes appearing to correlate with transitions between logged formations. Silicon is in higher concentrations from the top of the Waiora Formation with depth down hole displaying a clear break at the boundary of the Huka Falls and Waiora Formations, reflecting the change in lithology between lake sediments and volcaniclastic rocks. Potassium displays two clear changes in concentration down hole, a major change at 1040m where K ppm increases in the middle of the Waiora 1 ignimbrite (Wa1) which correlates with a recognised feed zone and a minor break at 330m where the Huka Formation transitions into the underlying volcaniclastic rocks. Changes in calcium concentration with depth are similar to K and mirrors that of Sr (Fig. 5c). Rubidium displays a clear break at 1040m where Rb is elevated in concentration (at the same location as the recognised feed zone, Contact Energy Ltd).

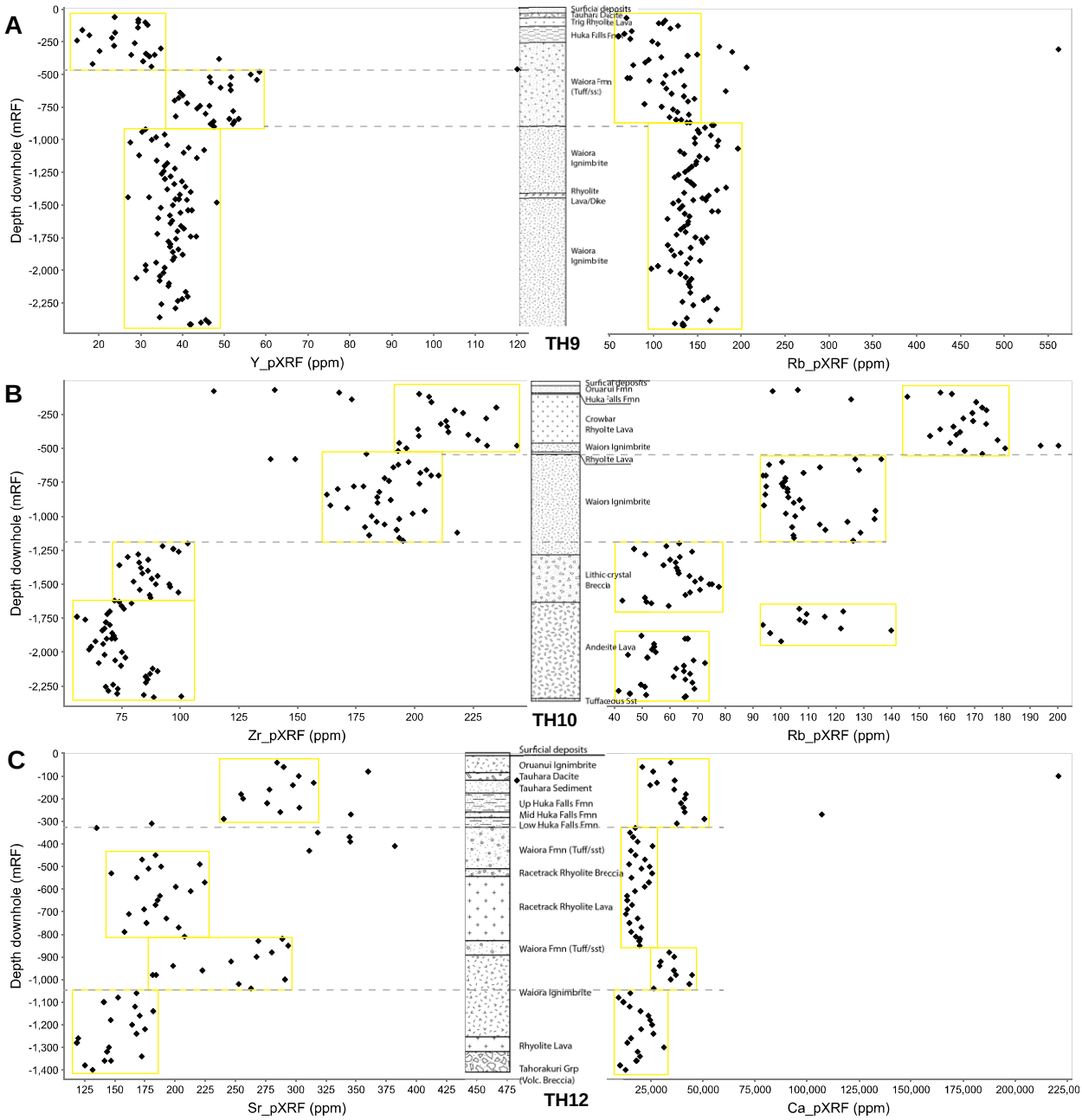

Figure 4: a) TH9, Y and Rb concentration, b) TH10, Zr and Rb concentration, c) TH12, Sr and Ca concentration. The concentrations of the selected elements shown commonly correlate with the different formations.

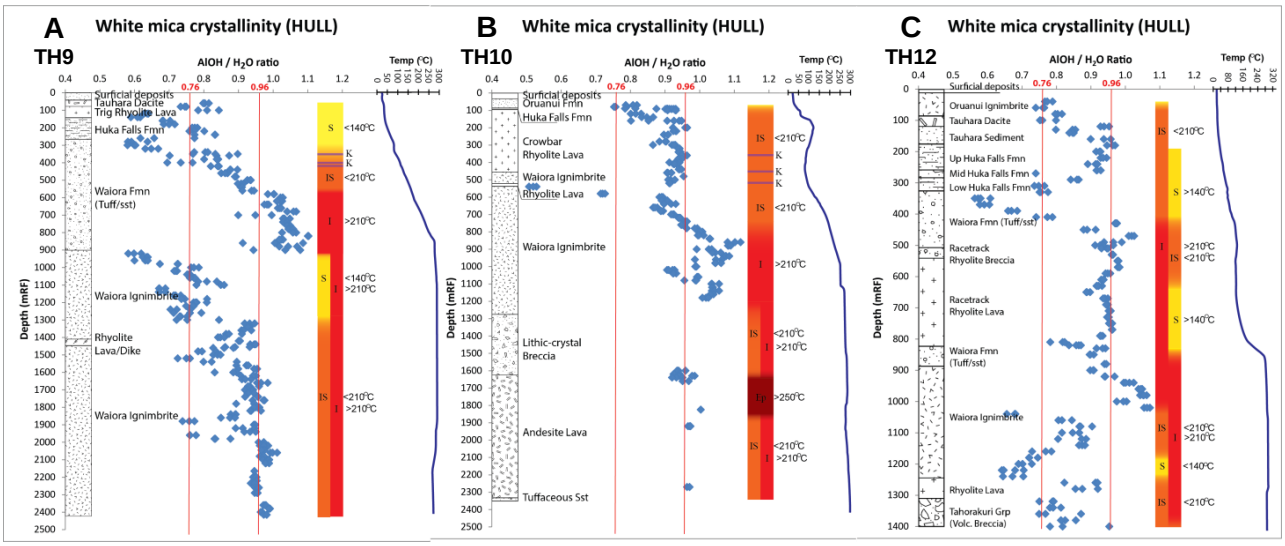

Figure 6: Red column is inferred mineral temperatures, the leftside is SWIR data; rightside is reported XRD data. K= kaolinite, S=smectite, IS=illite-smectite, I=illite, Ep = epidote. Blue line is measured well temperatures a) TH9 - 30 day heat up, b) TH10 - 28 day heat up and c) TH12 – 4 weeks heat up (Data from Contact Energy Ltd).

5. SWIR RESULTS

5.1. TH9 well

From 60 – 320 mRF in TH9 smectite dominates with illite-smectite from 340 – 540 mRF (Fig. 6a). Kaolinite is distinct at 350 mRF and is also present at 400 and 420 mRF where it is recognised in profiles by a subtle asymmetry. Illite predominates from 560 – 900 mRF along with minor chlorite and suspected calcite. From 920 – 1280 mRF the SWIR spectra resembles the profile of smectite. Cuttings from 1300 – 2415 mRF have illite-smectite/illite together with common chlorite and calcite. From 920-1280 mRF SWIR profiles have the appearance of smectite but XRD indicates illite. The contradictory spectra are dominated by a water feature suggesting the presence of additional water (possibly from fluid inclusions) that has resulted in a SWIR mis-identification. Further work is presently underway to better determine the source of the excess water in the SWIR profiles and to recognise spectral characteristics that could be used to distinguish when excess water is an issue.

5.2. TH10 well

Interlayered illite-smectite prevails over 70 – 760 mRF in TH10 (Fig. 6b) with rare kaolinite appearing at 360, 460 and 520 mRF. From 620 mRF chlorite and calcite appear with illite present from 740 – 1180 mRF. Strong calcite and chlorite dominate from 1200 – 2332 mRF and illite-smectite or illite is suspected to also be present in these samples, but is only seen as a subtle asymmetry obscured by strong spectral responses for chlorite and calcite. Only some samples below 1200 mRF have stronger profiles and appear mostly to be of illite. Epidote is identified in samples below 1640 mRF and is reported from binocular observation as present in low concentrations.

5.3. TH12 well

In well TH12 (Fig. 6c) illite-smectite dominates from 40 – 410 mRF. Generally illite with local illite-smectite occurs over 420 – 1020 mRF. Interlayered illite-smectite predominates from 1040 – 1400 mRF onwards with local apparent smectite around 1200 mRF. Below 1040 mRF chlorite and associated calcite are present. Below 1040 mRF the clay identified by SWIR is illite-smectite / smectite, but from XRD is illite. Again, SWIR spectra appear to have excess water (fluid inclusion / intra-crystalline) resulting in the mis-identification of illite.

5.4. Comparison of alteration mineralogy and known hydrothermal conditions

The distinction between smectite, illite-smectite and illite is based on the determination of the AlOH / H_2O ratio (white mica crystallinity). According to Simpson et al., (2013) the hull quotient ratio for AlOH / H_2O has an accuracy of 94%. The boundaries are <0.76 for smectite, interlayered illite-smectite is 0.76 and 0.96 and illite is >0.96. This generally distinguishes the clays but there can be some overlap, for example illite-smectites with a high percentage of illite can be categorized as illite. Figs 6a, b and c present hull quotient ratio boundaries (red lines) and illustrate the distribution of smectite, illite-smectite, illite and epidote down well, and can be used to infer the temperatures of hydrothermal fluids that formed these minerals (Browne, 1978). Smectite generally forms at temperatures of <150ºC, illite-smectite 150 – 210ºC, illite >210ºC and epidote >250ºC (Browne and Ellis, 1970). In TH9 there is a sequence of smectite to illite-smectite to illite with increasing depth and in TH10 and TH12 a general sequence of illite-smectite to illite. Both indicate a prograde sequence with depth. However in TH9 (920 – 1300 mRF) and also TH12 (below 1050 mRF) the interpretations of SWIR spectra suggest smectite or illite-smectite in contrast to illite identified from XRD.

The discrepancies between SWIR (smectite) and XRD (illite) could infer two different formation temperatures (Fig. 6c) as illite-smectite and illite formation temperatures are either <210ºC or >210ºC (Browne, 1978), so resolving this inconsistency is required. Measured well temperatures of >240°C below ~772 mRF and >280°C above ~952 mRF do not correlate with mineral assemblages identified by SWIR but are in agreement with Rosenberg et al., (2010) where the presence of epidote, wairakite, adularia and albite were noted, implying permeable conditions and formation temperatures of at least 240°C (Browne and Ellis, 1970).

The appearance of illite-smectite at the top of TH12 and TH10 suggests formation temperatures of <210°C, leading to an increase in formation temperature (>220°C) down well with the presence of illite (Browne, 1978). In TH12 formation temperatures seem to decrease to <210°C (Browne and Ellis, 1970) as illite-smectite appears then decreases further to <140°C (Browne and Ellis, 1970) from an interval of smectite-dominated rock at ~1200 mRF. The alteration mineralogy at depth is not consistent with the measured well temperature (280°C) in TH12 at ~820 m depth implying that fluid temperatures may have only recently increased because the smectite and illite-smectite should have transformed to illite at the modern fluid temperature. In TH12, but more obviously in TH10 due to the presence of epidote, the hydrothermal alteration appears to increase in intensity from an argillic to a propylitic alteration type down well, from a hydrothermal mineral assemblage of illite-smectite / illite, chlorite, epidote and calcite. Epidote occurrence implies formation temperatures of >250°C (Rosenberg et al., 2010). TH10 mineral inferred temperatures seem to generally correlate with measured well temperatures.

6. CONCLUSION

6.1. Efficacy of pXRF and SWIR in geothermal research

pXRF seems able to distinguish formation boundaries related to changes in lithology, based on marked changes in the concentrations of high field strength elements (HFSE) such as Y, Zr and Nb that have relatively low solubility in hydrothermal fluids. In addition, some other major elements such as Si also seem to correlate with variations in lithology. It is worth noting that boundaries are not always obvious from geological logging due to intense texturally destructive hydrothermal alteration. Therefore these can be refined from geochemistry such as pXRF, where distinct changes occur in the concentration of elements down hole (such as the change in concentration of various elements, including Zr, that occur in TH10 between 1180 and 1200m, Fig. 5b).

The concentration of some relatively mobile elements, such as Ba, K, Ca, As, and Rb also appear to correlate to formation boundaries. However there are some distinct variations in the concentrations of these elements which do not coincide with recognised formation boundaries, instead corresponding better with known areas of fluid flow (feed zones). Therefore recognition of changes in the concentration of these elements within rock types could be used to identify zones of hydrothermal fluid flow.

SWIR is a useful rapid technique however there are some issues with mis-identification that is currently being further investigated, subsequently this technique should be done in calibration with XRD to validate.

Nevertheless, utilising pXRF in geothermal research may save time and money when well logging because:

- It is reliable for measuring many elements (both HFSE and LILE) in hydrothermal cuttings which don't need to be prepared beyond being washed and dried.
- Lithological boundaries identified by logging are also characterized by changes in concentrations of various elements. By identifying lithogeochemical variations, pXRF is able to distinguish formations (particularly in areas where the lithologies are well known) and could also be used to identify hydrothermal feed zones.
- It is fast and rapid enough, that it could be used in real time to assess which formation the rig is currently drilling through.
- Sample preparation is faster, and the analytical method is inexpensive e.g. both the pXRF and SWIR probes can be placed directly onto cuttings

ACKNOWLEDGEMENTS

We would like to acknowledge Contact Energy for access to the drill cutting samples and thank Sophie Milloy and Fabian Sepulveda for their helpful review of the manuscript and constructive comments, GNS for their assistance and contribution, and The Sir Hugh Kawharu Foundation, AUSIMM and The Todd Academic Awards for Excellence for making this research possible.

REFERENCES

Bibby, H. M., Caldwell, T. G., Davey, F. J. and Webb, T. H. Geophysical evidence on the structure of the Taupo Volcanic Zone and its hydrothermal circulation. *Journal of Volcanology and Geothermal Research, 68:* 29-58. (1995).

Bignall, G., Milicich, S., Ramirez, E., Rosenberg, M., Kilgour, G. and Rae, A. Geology of the Wairakei-Tauhara geothermal system, New Zealand. *Proc. World Geothermal Congress 2010*, Bali, Indonesia (2010).

Bromley, C., Currie, S., Ramsay, G., Rosenberg, M., Pender, M., O'Sullivan, M. and Garvey, J. *Tauhara Stage II Geothermal Project: Subsidence Report*. GNS Science Consultancy Report 2010/151, pp. 154. (2010).

Browne, P.R.L. Hydrothermal alteration as an aid in investigating geothermal fields. *Geothermics 2*. (1970).

Browne, P.R.L. and Ellis, A.J. The Ohaaki-Broadlands hydrothermal area, New Zealand: Mineralogy and related geochemistry. *American Journal of Science 269*: 97-131. (1970).

Browne, P.R.L. Hydrothermal alteration in active geothermal fields. *Annual Review of Earth and Planetary Sciences 6*: 229-250. (1978).

Elliot, W. and Matisoff, G. Evaluation of kinetic models for the smectite to illite transformation. *Clays and Clay Minerals 44:* (1), 77-87. (1996).

Grange, L.I. *The geology of the Rotorua-Taupo subdivision, Rotorua and Kaimanawa divisions*. DSIR Geological Survey Branch, Bulletin Government Printer, Wellington. (1937).

Grange, L.I. *Geothermal steam for power in New Zealand*. Department of Scientific and Industrial Research, Wellington, New Zealand, Bulletin 117, 15–19pp. (1955).

Gravley, D.M., Wilson, C.J.N., Rosenberg, M.D. and Leonard G.S. The nature and age of Ohakuri Formation and Ohakuri Group rocks in surface exposures and geothermal drillhole sequences in the central Taupo Volcanic Zone, New Zealand. *New Zealand Journal of Geology and Geophysics 49:* 305-308. (2006).

Grindley, G.W. *The geology, structure and exploitation of the Wairakei Geothermal Field, Taupo*, New Zealand. New Zealand Geological Survey, Wellington, New Zealand, Bulletin 75, 131 pp. (1965).

Grindley, G. W. *Minerals of New Zealand, NZGS 38, Part D Geothermal Resources*, Tauhara Geothermal Field Report. New Zealand Geological Survey. (1974).

Grindley, G.W. The deeper structure of theWairakei geothermal field. *Proc. of the Pacific Geothermal Conference 1982*, University of Auckland, Auckland, New Zealand, pp. 69–74. (1982).

Healy, J. *Final logs – Holes TH1–TH4 Tauhara geothermal field*. New Zealand Geological Survey, unpublished Geothermal Circular JH7, Lower Hutt, New Zealand, 16 pp. (1967).

Henley, R. W. and Stewart, M. K. Chemical and isotopic changes in the hydrology of the Tauhara geothermal field due to exploitation at Wairakei. *Journal of Volcanology and Geothermal Research 15*: 285-314. (1983).

Hickey, K.A., Barker, S.L.L.B., Dipple, G.M., Arehart, G.B. and Donelick, R.A. The brevity of hydrothermal fluid flow revealed by thermal halos around giant gold deposits: Implications for Carlin-type gold systems. *Economic Geology 109:* 1461–1487. (2014).

Hunt, T.M., and Graham, D.J. Gravity changes in the Tauhara sector of the Wairakei-Tauhara geothermal field, New Zealand. *Geothermics 38*: 108–116. (2009).

Milloy, S.M., and Wei Lim, Y. Wairakei-Tauhara pressure regime update. *Proc. 34th New Zealand Geothermal Workshop 2012*, New Zealand. (2012).

Rosenberg, M., Wallin, E., Bannister, S., Bourguignon, S., Sherburn, S., Jolly, G. and Links, F. *Tauhara Stage II Geothermal Project*: Geoscience Report. GNS Science Consultancy Report 2010/138, pp. 318. (2010).

Shanks III, W.C.P. *Hydrothermal alteration in volcanogenic massive sulfide occurrence model.* U.S. Geological Survey Scientific Investigations Report 2010-5070-C/11, 12 p. (2012).

Simpson, M.P., Rae, A.J., Ganefianto, N., and Sepulveda, F. Short wavelength infrared (SWIR) spectral characterisation of smectite, illite-smectite and illite for geothermal fields of the Taupo Volcanic Zone, New Zealand. *Proc. 35th New Zealand Geothermal Workshop 17 – 20 November 2013*, Rotorua, New Zealand. (2013).

Simmons, S.F. and Brown, K.L. The flux of gold and related metals through a volcanic arc, Taupo Volcanic Zone, New Zealand. *Geology: 35* (12), 1099–1102. (2007).

Steiner, A. *The Wairakei Geothermal Area, North Island, New Zealand: its subsurface geology and hydrothermal rock alteration*. New Zealand Geological Survey, Bulletin 90, 134 pp. (1977).

Wilson, C.J.N. Stratigraphy, chronology, styles and dynamics of late Quaternary eruptions from Taupo volcano. *Philosophical Transactions of the Royal Society*, London A343, 205-306. (1993).

Wilson, C.J.N. The 26.5 ka Oruanui eruption, New Zealand: an introduction and overview. *Journal of Volcanology and Geothermal Research 112:* 133-174. (2001).